

Comparison of Adaptive Kalman Filters in Aircraft State Estimation

MERT SEVER¹, TUNCAY YUNUS ERKEÇ¹, CHINGIZ HAJIYEV²

¹Atatürk Strategic Studies, and Graduate Institute,
Turkish National Defense University,
Levent, 34334, Istanbul,
TURKEY

²Faculty of Aeronautics and Astronautics,
Istanbul Technical University,
Ayazağa, 34469, Maslak, Istanbul,
TURKEY

Abstract: - Aircraft state estimation refers to the process of determining the current or future state of an aircraft, such as its position, velocity, orientation, and other relevant parameters, based on available sensor data and mathematical models. This information is crucial for safe and efficient flight operations, as well as for various applications, including Guidance, Navigation, Control (GNC), and autonomous flight. Given the beginning circumstances, the motion of the airplane was examined in this study by estimating the state vectors using the Kalman Filter (KF) and the Adaptive Kalman Filters (AKF), as well as by comparing the various estimate techniques.

Key-Words: - Aircraft, State Vectors, Kalman Filters, Flight Dynamics

Received: June 19, 2022. Revised: August 23, 2023. Accepted: September 25, 2023. Published: October 30, 2023.

1 Introduction

State estimation can be a challenging task due to the complexity of the aircraft dynamics, sensor limitations, and environmental factors. Advances in sensor technology and estimation algorithms have improved the accuracy and reliability of state estimation in modern aircraft, contributing to safer and more efficient flight operations, [1].

Key components of aircraft state estimation include:

Sensor Data: Aircraft are equipped with various sensors, such as GPS (Global Positioning System), inertial measurement units (IMUs), altimeters, airspeed indicators, and more. These sensors provide data on the aircraft's physical state and environment.

Mathematical Models: To estimate the aircraft's state accurately, mathematical models are used. These models incorporate the principles of physics and aerodynamics to predict how an aircraft's state will evolve. These models may include equations of motion, atmospheric models, and sensor error models.

Sensor Fusion: Since no single sensor is perfect and sensor measurements can be noisy or subject to errors, sensor fusion techniques are employed to combine data from multiple sensors. Kalman filters

and extended Kalman filters are commonly used for this purpose.

Filtering and Smoothing: Estimation methods often involve filtering techniques, which provide real-time estimates of the aircraft's state as new sensor data becomes available. Smoothing techniques, on the other hand, are used to refine the state estimates using historical data.

Navigation: State estimation is fundamental to aircraft navigation. It enables the aircraft to determine its position and orientation accurately, helping it follow a desired flight path, avoid obstacles, and maintain proper altitude.

Control: Aircraft state estimation is critical for flight control systems. By knowing the aircraft's state, the control system can adjust, ensure stability, respond to pilot inputs, and execute various flight maneuvers.

Autonomous Flight: In the context of autonomous flight, state estimation plays a crucial role in enabling drones, UAVs (Unmanned Aerial Vehicles), and autonomous aircraft to operate safely and perform complex missions without direct human intervention.

Safety and Redundancy: Aircraft state estimation is an essential component of safety-critical systems. Redundant sensors and estimation algorithms are often employed to ensure that the aircraft can

continue to operate safely in the event of sensor failures or other anomalies.

In addition, numerous approaches for estimating aircraft state vectors are being worked on. For the estimate of motion state vectors for various platforms than airplanes, Kalman filters (KF) and state vector estimations have demonstrated their effectiveness and excel in terms of their high accuracy, [2], [3], [4], [5], [6].

The Extended Kalman Filter (EKF) is a widely used technique for state estimation in the presence of noise and disturbances. However, as mentioned before, it can face challenges when dealing with practical usage where system and sensor noises occur. In such cases, the Adaptive Kalman Filter (AKF) has gained popularity for its ability to handle varying noise and improve state estimates in the presence of disturbances.

Here is an overview of the AKF and its advantages:

Adaptability: The key advantage of the AKF over the standard EKF is its adaptability. The AKF can adjust its filter parameters (such as process and measurement noise covariance matrices) based on the evolving noise and uncertainties in the system. This adaptability allows the filter to respond to changing conditions and provide more accurate state estimates.

Handling Changing Noise Levels: In practical applications, the levels of system and sensor noise can change over time due to various factors such as environmental conditions, sensor degradation, or system component wear and tear. The AKF is designed to continuously update its noise models, ensuring that it can effectively estimate the state even when noise levels are not constant.

Robustness: By adapting to changing noise characteristics, the AKF can provide more robust and accurate state estimation in challenging environments. It can effectively deal with disturbances and sensor noise that may cause problems for traditional fixed-parameter filters like the EKF.

Improved Convergence: The adaptability of the AKF can help improve convergence and reduce the time it takes for the filter to provide accurate state estimates, especially in situations where noise levels change rapidly or unpredictably.

Reduced Tuning Requirements: Unlike traditional Kalman filters, which often require manual tuning of the noise covariance matrices, the AKF reduces the need for extensive tuning. This can be particularly advantageous in scenarios where obtaining accurate noise models is challenging.

Real-Time Applications: The AKF is well-suited for real-time applications, including autonomous navigation, robotics, and aviation, where adaptability and robustness are critical for safe and accurate operation, [7].

It is important to note that the choice between the EKF and the AKF depends on the specific requirements and characteristics of the system, as well as the nature of the noise and disturbances encountered in practical applications. The AKF's adaptability can be an asset in scenarios where noise levels are dynamic and not easily predictable, making it a suitable choice for applications where maintaining accurate state estimates is essential.

A novel multiple fading factors Kalman filtering technique is provided in the research "Multiple Fading Factors Kalman Filter for SINS Static Alignment Application" by, [8]. The fading factor matrix is created by computing the unbiased estimate of the innovation sequence covariance using fenestration. The technique offers various rates of fading for various filter channels by adjusting the covariance matrix of prediction error and fading factor matrix. The strap-down inertial navigation devices are used using the suggested approach. It is discovered that the suggested technique has superior parameter estimation in real-world settings and is more effective against noise.

A further work, [9], examined the same topic. A sequential technique is presented to concurrently calculate the orbit and attitude of a small spacecraft based on magnetometer and gyro measurements, [9]. A robust adaptive Kalman filter is developed to reduce the effect of orbital errors on attitude prediction.

For altering the measurement covariance matrix \mathbb{R} , Almagbile, Wang, and Al-Rawabdeh examined the Sage Husa adaptive Kalman filter (SHAKF) and innovation-based adaptive Kalman filter (IAKF) techniques, [10].

A strong tracking variational Bayes adaptive Kalman filter based on multiple damping factors was proposed by Pan and colleagues in a study that was published in 2020, [11]. This filter takes into account the fact that if the system model or the statistical properties of the noise are inaccurate, past measurements will directly affect the accuracy of the current state estimation and may even lead to filtering bias.

The system errors have been increased beyond the predetermined simulation duration, and the filters' responses to the faults were observed. In the event of a potential rise in inaccuracy in the systems, it was attempted to show which filter produced superior outcomes.

In this study, the scaling adaptive Kalman filter, residual adaptive Kalman filter, and conventional Kalman filter are compared for the single and double-sensor fault scenarios applied to aircraft dynamics.

2 Problem Formulation

In this part, the mathematical model of the motion of the aircraft is explained.

Longitudinal motion, [12].

$$\dot{X}_{long} = \begin{bmatrix} X_u & X_w & 0 & -g \cos \chi_0 \\ Z_u & Z_w & U_0 & -g \sin \chi_0 \\ \bar{M}u & \bar{M}w & \bar{M}q & \bar{M}\Theta \\ 0 & 0 & 1 & 0 \end{bmatrix} \cdot X_{long} + \begin{bmatrix} X_{\delta E} \\ Z_{\delta E} \\ \bar{M}_{\delta E} \\ 0 \end{bmatrix} \cdot u \quad (1)$$

$$X_{long}^T = [u \quad w \quad q \quad \Theta] \quad (2)$$

Here, u longitudinal velocity, w vertical velocity, q pitch velocity, Θ pitch angle and δ_E is the tilt angle of the elevator.

$$u = [\delta_E] \quad (3)$$

$$\dot{X}_{long} = A \cdot X_{long} + B \cdot u \quad (4)$$

$$\bar{M}u = Mu + \bar{M}w \cdot Zu$$

$$\bar{M}w = Mw + \bar{M}w \cdot Zu$$

$$\bar{M}q = Mq + U_0 \cdot \bar{M}w \quad (5)$$

$$M\Theta = -g \cdot Mw \cdot \sin \chi_0$$

$$\bar{M}_{\delta E} = M_{\delta E} + \bar{M}w \cdot Z_{\delta E}$$

Latitudinal motion, [12].

$$\dot{X}_{lat} = \begin{bmatrix} Y_v & 0 & -1 & \frac{g}{U_0} \\ L'_\beta & L'_p & L'_r & 0 \\ N'_\beta & N'_p & N'_r & 0 \\ 0 & 1 & \tan \chi_0 & 0 \end{bmatrix} \cdot X_{lat} + \begin{bmatrix} 0 & Y_{\delta R}^* \\ L'_{\delta A} & L'_{\delta r} \\ N'_{\delta A} & N'_{\delta r} \\ 0 & 0 \end{bmatrix} \cdot \begin{bmatrix} \delta_A \\ \delta_R \end{bmatrix} \quad (6)$$

$$X_{lat} = [\beta \quad p \quad r \quad \phi]^T \quad (7)$$

Here, β is the yaw angle, p is the roll angular velocity, r is the yaw angular velocity, ϕ is the roll angle.

The longitudinal and latitudinal state vectors can be obtained as follows

$$X = [u \quad w \quad q \quad \Theta \quad \beta \quad p \quad r \quad \phi]^T \quad (8)$$

The longitudinal and latitudinal system matrices are combined as following

$$A = \begin{bmatrix} A_{long} & 0 \\ 0 & A_{lat} \end{bmatrix} \quad (9)$$

The combined control vector is,

$$u = \begin{bmatrix} \delta_E \\ \delta_A \\ \delta_R \end{bmatrix} \quad (10)$$

where δ_A and δ_R are the tilt angles of the ailerons and rudder respectively

The combined control distribution matrix,

$$B = \begin{bmatrix} B_{long (4x1)} & 0_{4x2} \\ 0_{4x1} & B_{lat (4x2)} \end{bmatrix} \quad (11)$$

The equation of aircraft full motion can be written in the form as follows.

$$\dot{X} = A \cdot X + B \cdot u$$

After the discretization of Eq. (12) we have

$$\dot{X}_i = \frac{X_{i+1} - X_i}{\Delta t} = A \cdot X_i + B \cdot u \quad (13)$$

$$X_{i+1} - X_i = \Delta t \cdot A \cdot X_i + \Delta t \cdot B \cdot u \quad (14)$$

After mathematical transformations, the mathematical model of the motion of the aircraft was obtained as

$$X_{i+1} = (I + \Delta t \cdot A)X_i + \Delta t \cdot B \cdot u \quad (15)$$

Substituting

$$A^* = (I + \Delta t \cdot A) \quad (16)$$

$$B^* = (\Delta t \cdot B) \quad (17)$$

into equation 15, we can obtain the mathematical model of the motion of aircraft as follows.

$$X_{i+1} = A^*X_i + B^*u \quad (18)$$

3 Kalman Filter for Aircraft State Estimation

Kalman Filter is an estimation approach for linear systems, [13]. As the model is linear, by processing noisy measurements, KF estimates the state vectors with high accuracy.

Estimation equation of the filter

$$\hat{x}(k/k) = \hat{x}(k/k-1) + K(k)\bar{z}(k) \quad (19)$$

The extrapolation equation is shown as

$$\hat{x}(k/k-1) = A^* \hat{x}(k-1/k-1) + B^* \cdot u \quad (20)$$

Innovation sequence

$$\bar{z}(k) = Z(k) - H\hat{x}(k, k-1) \quad (21)$$

$Z(k)$ is the measurement vector. Kalman gain matrix can be expressed as

$$K(k) = P(k/k-1)H^T(HP(k/k-1)H^T + R)^{-1} \quad (22)$$

Predicted covariance matrix of estimation error,

$$P(k/k-1) = A^*P(k-1/k-1)A^{*T} + G(k, k-1)Q(k-1)G(k, k-1)^T \quad (23)$$

Here Q is the system noise covariance matrix. The covariance matrix of Estimation error is,

$$P(k/k) = (I - K(k)H(k))P(k/k-1) \quad (24)$$

Measurement matrix

$$H = I_{8 \times 8} \quad (25)$$

Measurement error covariance matrix

$$R = \begin{bmatrix} \sigma_u^2 & 0 & 0 & 0 & 0 & 0 & 0 & 0 \\ 0 & \sigma_w^2 & 0 & 0 & 0 & 0 & 0 & 0 \\ 0 & 0 & \sigma_q^2 & 0 & 0 & 0 & 0 & 0 \\ 0 & 0 & 0 & \sigma_\theta^2 & 0 & 0 & 0 & 0 \\ 0 & 0 & 0 & 0 & \sigma_\beta^2 & 0 & 0 & 0 \\ 0 & 0 & 0 & 0 & 0 & \sigma_p^2 & 0 & 0 \\ 0 & 0 & 0 & 0 & 0 & 0 & \sigma_r^2 & 0 \\ 0 & 0 & 0 & 0 & 0 & 0 & 0 & \sigma_\phi^2 \end{bmatrix} \quad (26)$$

Transition matrix of system noise

$$G(k, k-1) = I_{8 \times 8} \quad (27)$$

4 Adaptive Kalman Filter

4.1 Residual Adaptive Kalman Filter

The Residual Adaptive Kalman Filter is a filter that adaptably calculates the R matrices during the simulation. R matrix undergoes iterative alterations in contrast to KF. This enhancement makes the filter less susceptible to potential faults, [14].

Innovation

$$d(k) = [Z(k) - H\hat{x}(k/k-1)] \quad (28)$$

Estimation equation

$$\hat{x}(k/k) = \hat{x}(k/k-1) + K(k)d(k) \quad (29)$$

Residual

$$\varepsilon(k) = [Z(k) - H\hat{x}(k/k)] \quad (30)$$

Measurement error covariance matrix

$$R(k) = \alpha R(k-1) + (1-\alpha)x(\varepsilon(k)\varepsilon(k)^T + H(k)P(k/k-1)H(k)^T) \quad (31)$$

Kalman gain matrix,

$$K(k) = P(k/k-1)H^T(HP(k/k-1)H^T + R(k))^{-1} \quad (32)$$

Here, $\alpha = 0.3$ according to previous studies, [15]. The rest of the KF equations are the same as in the previous section.

4.2 Scaling Adaptive Kalman Filter

The multiple measurement noise scale factor technique has been found to produce superior outcomes in multivariate systems in earlier investigations. The technique of choice fixes the measurement noise-covariance matrix and Kalman gain using a matrix known as the scale factor, [15].

Scale matrix S(k) is incorporated into the method in contrast to the Kalman filter.

$$S(k) = \left(\frac{1}{\mu} \sum_{j=k-\mu+1}^k \bar{z}(k)\bar{z}(k)^T - H(k)P(k/(k-1)H^T(k)) \right) R^{-1} \quad (33)$$

Here μ is the width of the moving window. The diagonal elements of the scale matrix may not be less than one, so the following rule is suggested to avoid this situation.

$$S^* = \text{diag}(s_1^*, s_2^*, s_3^*, \dots, s_n^*) \quad (34)$$

and,

$$s_i^* = \max\{1, s_{ii}\} \quad i = 1, n \quad (35)$$

Here s_{ii} represents the i 'th diagonal element of the matrix S(k). By using scale factor Kalman gain matrix can be expressed as,

$$K(k) = P(k/k-1)H^T(HP(k/k-1)H^T + S^*(k)R)^{-1} \quad (36)$$

As with section 3, the remaining Kalman filter formulas are identical. Any system fault increases the corresponding diagonal matrix element. Scale factor increases lower the Kalman gain and the impact of innovation on the state update process. With this concept, estimates may be obtained with more accuracy, [16].

5 Simulation Results and Discussion

In this study, the motion of the aircraft is simulated by using MATLAB. The measurement vector is,

$$Z = [Z_u \ Z_w \ Z_q \ Z_\theta \ Z_\beta \ Z_p \ Z_r \ Z_\phi]^T \quad (37)$$

The measurements are simulated via the formulas below,

$$\begin{aligned} Z_u &= u + \sigma_u \cdot \text{randn} \\ Z_w &= w + \sigma_w \cdot \text{randn} \\ Z_q &= q + \sigma_q \cdot \text{randn} \\ Z_\theta &= \theta + \sigma_\theta \cdot \text{randn} \\ Z_\beta &= \beta + \sigma_\beta \cdot \text{randn} \\ Z_p &= p + \sigma_p \cdot \text{randn} \\ Z_r &= r + \sigma_r \cdot \text{randn} \\ Z_\phi &= \phi + \sigma_\phi \cdot \text{randn} \end{aligned} \quad (38)$$

Here σ is the standard deviation of the measurement error.

$$\begin{aligned} \sigma_u = \sigma_w = 0.92m, \sigma_q = \sigma_p = \sigma_r = 0.0083 \text{ rad}, \\ \sigma_\theta = \sigma_\phi = 0.017 \text{ rad and } \sigma_\beta \\ = 0.005 \text{ rad}. \end{aligned}$$

After a specified time, it's simulated that the pitch angle sensor and roll rate sensor were broken.

5.1 Single Sensor Fault Results

Cases involving pitch angle fault and roll rate fault are covered individually. State vector and scale factor graphs for each normalized innovation under each case are shown.

5.1.1 Noise Increment Fault Scenario

In this scenario, to simulate faulty measurements, σ_θ and σ_p are multiplied by 50 for each case.

i) Noise Increment Type Pitch Angle Gyro Fault

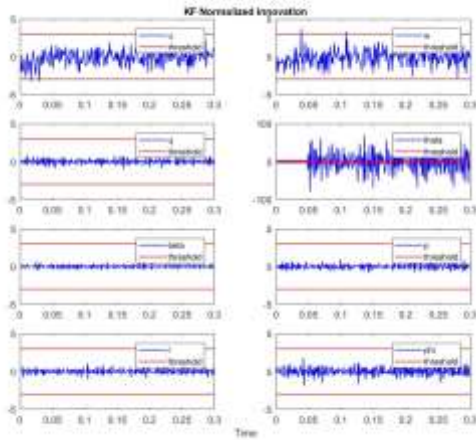


Fig. 1: Conventional KF normalized innovations in the presence of pitch angle gyro noise increment fault

As shown in Figure 1, because of the fault on the pitch angle gyroscope, after 0.05 seconds, the normalized innovation of the pitch angle (theta) exceeds the threshold which is ± 3 .

Pitch angle estimation results and pitch angle scaling factor graph in the case of noise increment fault are given in Figure 2 and Figure 3 respectively.

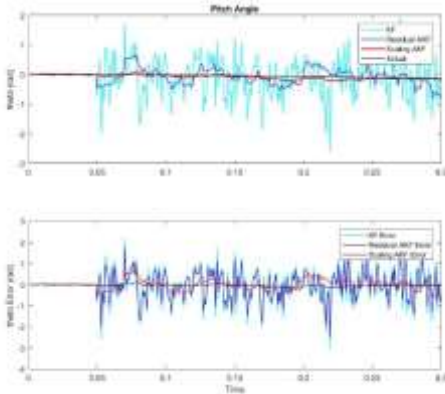


Fig. 2: Pitch angle estimation results in the presence of pitch angle gyro noise increment fault

The root mean square errors (RMSE) for pitch angle estimation in the presence of pitch angle gyro noise increment fault are given in Table 1.

Table 1. RMSE for pitch angle in the case of noise increment fault

Filter / State	KF	Residual AKF	Scaling AKF
Theta	0.711162	0.317198	0.040281

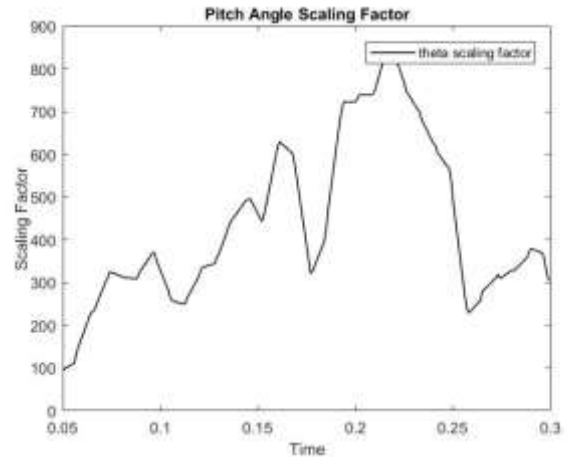


Fig. 3: Pitch angle scaling factor in the case of noise increment fault

The pitch angle scaling factor rises as a result of the pitch angle gyro fault, leading to more precise pitch angle calculations.

ii) Noise Increment Type Rate Gyro Fault

The conventional KF normalized innovation results for the case of roll rate gyro noise increment fault are given in Figure 4.

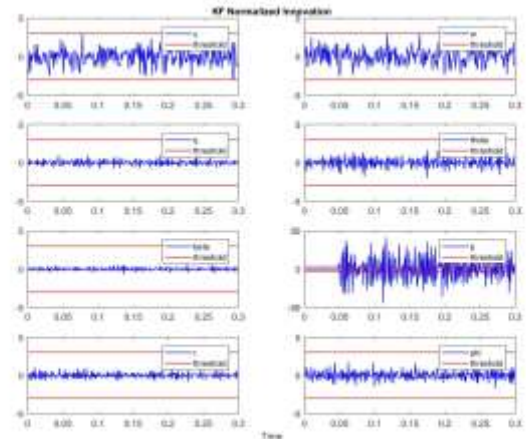


Fig. 4: Conventional KF normalized innovations in the presence of roll rate gyro noise increment fault

As can be seen in the figure, because of the fault on the roll rate gyroscope, after 0.05 seconds of simulation, the normalized innovation of the roll angle (p) exceeds the threshold which is ± 3 .

Figure 5, Figure 6 show the roll rate estimation results and roll rate scaling factor graph for the case of noise increment fault respectively. The scaling factor of the roll rate improves as a result of the roll rate gyro's fault, allowing for more precise roll rate calculations.

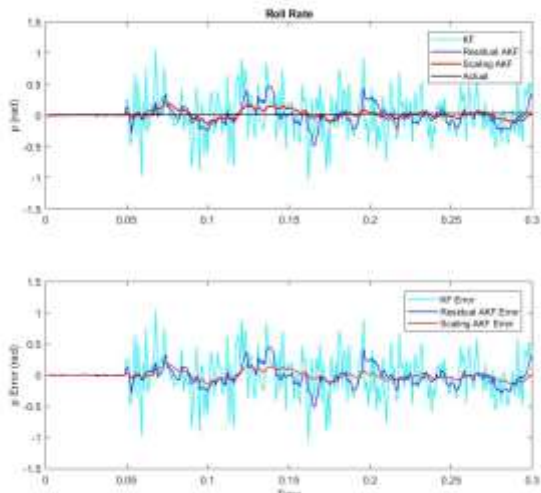


Fig. 5: Roll rate estimation results for noise increment fault case

The roll rate root mean square errors in the case of noise increment for KF, residual AKF, and scaling AKF are given in Table 2.

Table 2. RMSE for roll rate in the case of noise increment fault

Filter / State	KF	Residual AKF	Scaling AKF
p	0.364050	0.152013	0.074246

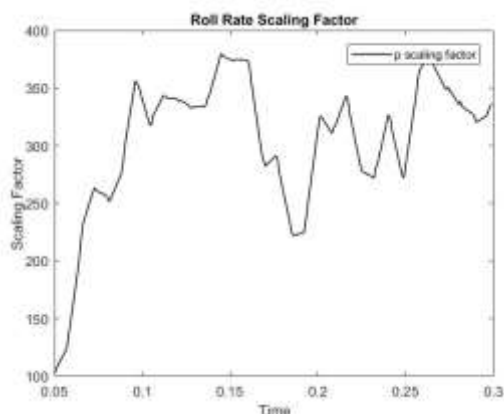


Fig. 6: Roll rate scaling factor graph for noise increment fault case

Scaling AKF is the most effective method for tolerating the system malfunction for noise increment faulty systems, as demonstrated by graphs and root mean square errors (Table 1, Table 2). Compared to KF, adaptive approaches produce

superior outcomes. Scaling AKF tolerates the system error in the system better than the residual AKF technique, according to comparisons between adaptive approaches.

5.1.2 Bias Noise Fault Scenario

In this scenario, to simulate faulty measurements, Z_{θ} and Z_p are summed with 0.1 radians for each case.

iii) Bias Noise Type Pitch Angle Gyro Fault

Pitch angle estimation results in case of bias noise are given in Figure 7.

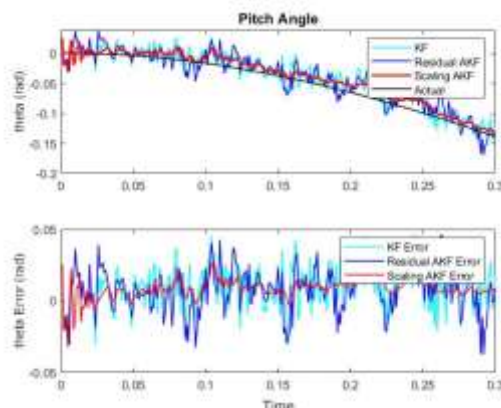


Fig. 7: Pitch angle estimation results in case of bias noise

The pitch angle root mean square errors under the condition of bias noise for KF, residual AKF, and scaling AKF are given in Table 3.

Table 3. RMSE for pitch angle in the case of bias noise fault

Filter / State	KF	Residual AKF	Scaling AKF
Theta	0.052242	0.050676	0.042016

iv) Bias Noise Type Roll Rate Gyro Fault

Roll rate estimation results in the case of bias noise fault are given in Figure 8.

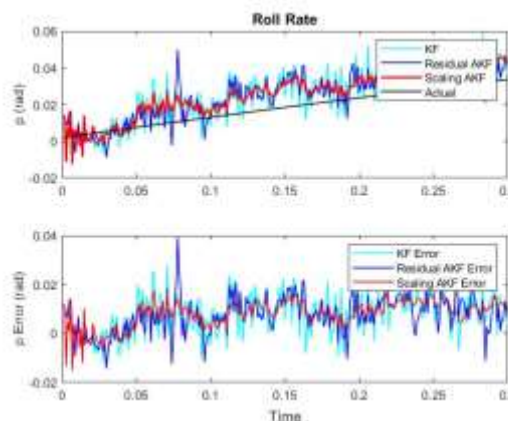


Fig. 8: Roll rate estimation results in the case of a bias noise fault

The roll rate root mean square errors under the condition of bias noise for KF, residual AKF, and scaling AKF are given in Table 4.

Table 4. RMSE for roll rate in the case of a bias noise fault

Filter / State	KF	Residual AKF	Scaling AKF
p	0.587203	0.510237	0.423295

Scaling AKF is the most effective method for tolerating system malfunction for bias noise faulty systems, as demonstrated by graphs and root mean square errors (Table 3, Table 4). Compared to KF, adaptive approaches give better estimations. When we rank the methods, scaling AKF achieved the best result while conventional KF achieved the worst result.

5.2 Double Sensor Fault Results

Pitch angle and roll rate sensors are faulty simultaneously in this manner. At the end of the specified time (0.05 seconds after the simulation starts), distortion is introduced to the pitch angle and rotation speed gyroscopes. Considering this situation, the following scenarios are applied.

- a. Noise increment fault for both sensors
- b. Bias noise fault for both sensors
- c. Noise increment fault for pitch angle gyro and bias noise fault for roll rate gyro

5.2.1 Noise Increment Fault for Both Sensors

In this scenario, to simulate faulty measurements, σ_θ and σ_p are simultaneously multiplied by 50.

Figure 9, Figure 10, Figure 11, Figure 12 and Figure 13 show the graphs for normalized innovation, state estimation, and scale factor respectively. Additionally, the RMSE results for the noise increment type double sensor faults are provided (Table 5).

Figure 9 presents the Conventional KF normalized innovations for the case of double noise increment sensor faults. Pitch angle gyro (θ) and roll rate gyro (p) were found to be greater than the threshold of 3 after the fault occurred at 0.05 seconds of the simulation.

Figure 10, Figure 12 and Figure 13 show the results of the pitch angle and roll rate estimations as well as scale factor graphs for the case of noise increment type sensor faults. The results indicated that the scaling factor grows as system malfunction increases.

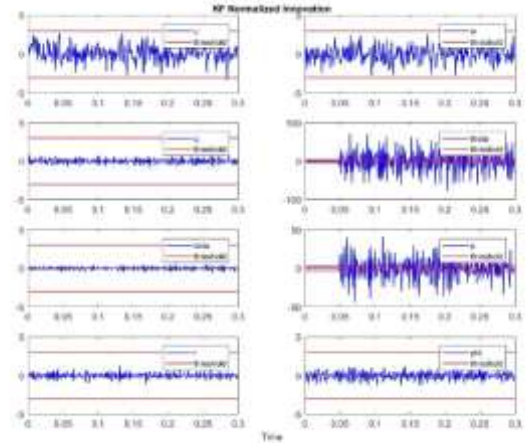


Fig. 9: Conventional KF normalized innovations for the case of noise increment type double sensor faults

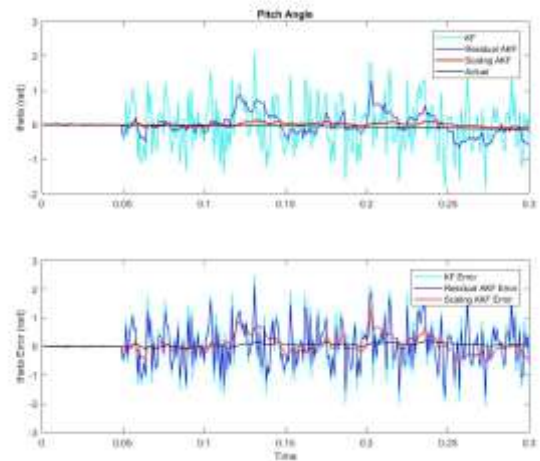


Fig. 10: Pitch angle estimation results for the case of noise increment type double sensor faults

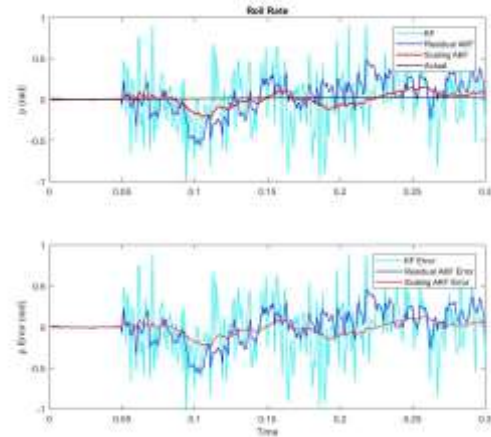


Fig. 11: Roll rate estimation results for the case of noise increment type double sensor faults

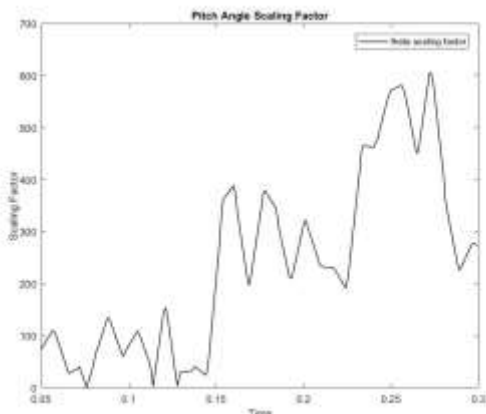


Fig. 12: Pitch angle scaling factor graph for the case of noise increment type double sensor faults

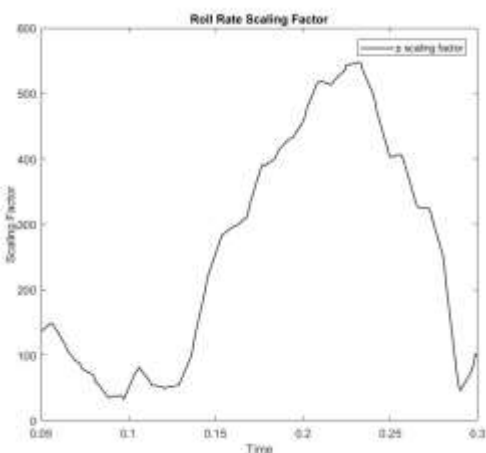


Fig. 13: Roll rate scaling factor graph for the case of noise increment type double sensor faults

Table 5 provides pitch angle and roll rate root mean square errors for each filter in the case of noise increment type double sensor faults scenario.

Table 5. RMSE of the pitch angle and roll rate in the case of noise increment type double sensor faults.

Filter / State	KF	Residual AKF	Scaling AKF
Theta	0.716393	0.201855	0.066984
p	0.371447	0.222162	0.073049

As demonstrated by plots (Figure 9, Figure 10, Figure 11, Figure 12, Figure 13) and root mean square errors (Table 5 and Table 6), scaling AKF is the best method for tolerating the failure in case of noise increment type double sensor fault. Adaptive approaches produce more precise estimates than traditional KF. Scaling AKF is more tolerant of the system flaw than other adaptive techniques.

5.2.2 Bias Noise Type Double Sensor Faults

In this scenario, to simulate faulty measurements, Z_θ and Z_p are simultaneously summed with 0.1 radians.

Figure 14, Figure 15 and Figure 16 show the graphs for state estimations. Additionally, the RMSE results for the bias noise type double sensor faults are provided (Table 6).

Figure 14 represents the pitch angle estimation results for the case of bias noise type double sensor faults.

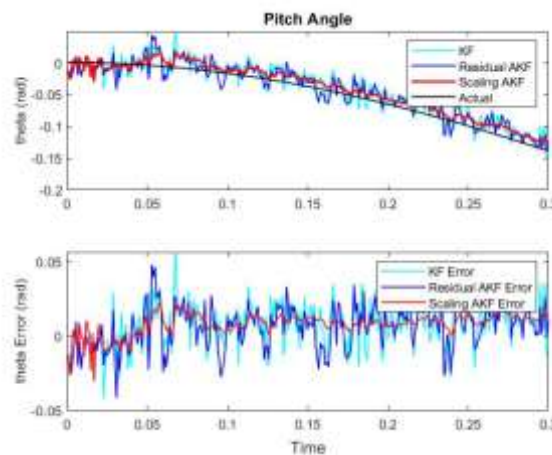


Fig. 14: Pitch angle estimation results for the case of bias noise type double sensor faults

Figure 15 represents the roll rate estimation results for the case of bias noise type double sensor faults.

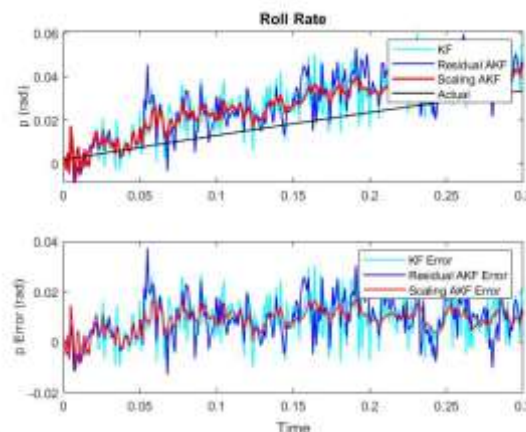


Fig. 15: Roll rate estimation results for the case of bias noise type double sensor faults

Table 6 provides pitch angle and roll rate root mean square errors for each filter for the scenario of bias noise type double sensor faults.

Table 6. RMSE of the pitch angle and roll rate for the bias noise type double sensor faults.

Filter / State	KF	Residual AKF	Scaling AKF
theta	0.151124	0.123794	0.098763
p	0.173246	0.132962	0.088937

5.2.3 Different Types of Double Sensor Faults

In this scenario, to simulate pitch angle gyro and roll rate gyro measurements, σ_{θ} multiplied by 50 and Z_p is summed with 0.1 radians.

Figure 16 presents the Conventional KF normalized innovations for the case of double sensor faults, noise increment fault for pitch angle gyro, and bias noise fault for roll rate gyro. The pitch angle gyro (θ) and roll rate gyro (p) are found to be greater than the threshold, which is 3. As seen, the normalized innovations of the pitch angle and roll angle channels exceed the threshold which is ± 3 after the fault occurs at 0.05 seconds of the simulation.

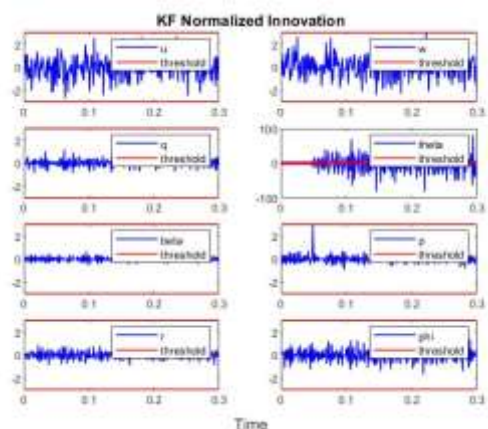


Fig. 16: Conventional KF normalized innovations for the case of double sensor faults (noise increment fault for pitch angle gyro and bias noise fault for roll rate gyro)

Figure 17 and Figure 18 represent the pitch angle and roll rate estimation results for the case of double sensor faults (noise increment fault for pitch angle gyro and bias noise fault for roll rate gyro).

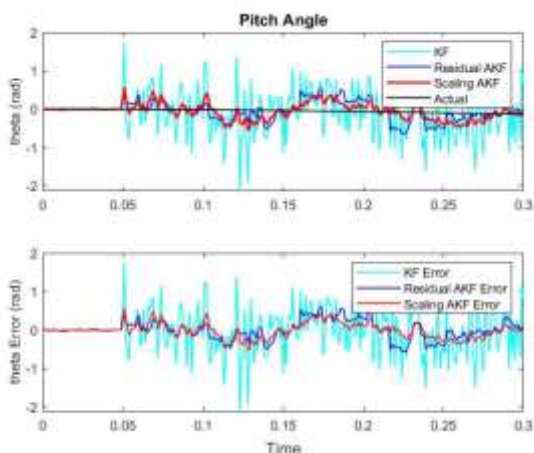


Fig. 17: Pitch angle estimation results for the case of double sensor faults (noise increment fault for pitch angle gyro and bias noise fault for roll rate gyro).

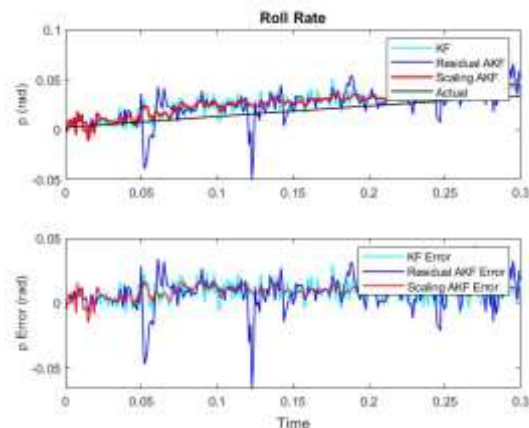


Fig. 18: Roll rate estimation results for the case of double sensor faults (noise increment fault for pitch angle gyro and bias noise fault for roll rate gyro).

Figure 19 and Figure 20 show the results of the pitch angle and roll rate estimations as well as scale factor graphs. According to the obtained results, the scaling factor increases as system malfunction increases.

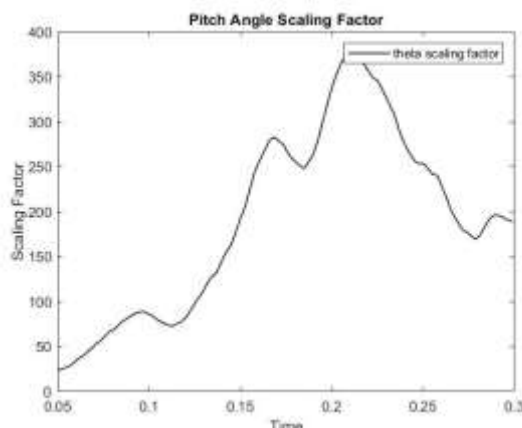


Fig. 19: Pitch angle scaling factor graph for the case of double sensor faults (noise increment fault for pitch angle gyro and bias noise fault for roll rate gyro).

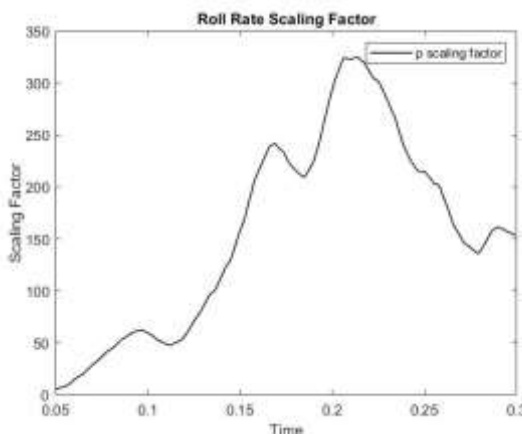


Fig. 20: Roll rate scaling factor graph for the case of double sensor faults (noise increment fault for pitch angle gyro and bias noise fault for roll rate gyro).

Table 7 provides pitch angle and roll rate root mean square errors for each filter in this scenario.

Table 7. RMSE of the pitch angle and roll rate for the double sensor faults (noise increment fault for pitch angle gyro and bias noise fault for roll rate gyro)

Filter / State	KF	Residual AKF	Scaling AKF
Theta	0.0.644407	0.264420	0.216585
p	0.0.012244	0.015997	0.010125

When both noise approaches are compared, it was found that noise increment is a more realistic approach than bias noise for simulating the system noise. The adaptive filters give better results for the noise increment type scenario. Moreover, the results revealed that scaling AKF is still the best filter for not only both noise increment and bias noise systems but also complex double-sensor fault systems.

Increasing the vector sensitivity is crucial for the direction control of fast-moving aircraft. An increase in mistakes in aircraft status detection and control is brought on by high-value error rates that may arise in the estimate of aircraft orientation states.

This study has established the significance of adopting the scaling AKF estimate technique rather than residual AKF and traditional KF, particularly in aircraft orientation and control systems with high noise ratios.

6 Conclusions

In this study, the motion of the airplane was examined by estimating the state vector using the Conventional Kalman Filter and Adaptive Kalman Filters and comparing various estimation techniques.

Utilizing the scaling adaptive Kalman filter, residual adaptive Kalman filter, and conventional Kalman filter, measurements were processed. Investigations were conducted into the single-sensor fault and double-sensor fault sensor failure scenarios. For both single-sensor fault and double-sensor fault scenarios, it was concluded that predicted results by scaling AKF are more accurate than those from the other two approaches.

Additionally, it was discovered that the KF and residual AKF errors rise when a system fault occurs, but the scaling AKF filter is adaptively self-adjusting and is not as significantly impacted by the increasing error as other systems. Scaling AKF estimate remains more stable as a result. After

scaling the AKF technique, residual AKF provides the second-best estimation.

This study may be used for UAV and aircraft missions to improve system accuracy. Additionally, it has been demonstrated via the use of this study that scaling the AKF allows for the tolerability of large system faults. The impact of KF and AKF approaches on multi-satellite flight issues will be investigated in the future.

References:

- [1] Erkeç, T.Y., and Hajiyev, C., Fault-tolerant state estimation methods of cluster satellites, *Advances in Space Research*, Vol. 71, 2023, pp.3868-3882.
- [2] Curvo, M., Estimation of aircraft aerodynamic derivatives using Extended Kalman Filter. *Journal of the Brazilian Society of Mechanical Sciences*, Vol. 22, 2000.
- [3] Soken, H., and Hajiyev, C., Robust Adaptive Kalman Filter for Estimation of UAV Dynamics in the Presence of Sensor/Actuator Faults. *Aerospace Science and Technology*, Vol. 28, 2013, pp.376–383.
- [4] Chowdhary, G., and Jategaonkar, R., Aerodynamic Parameter Estimation from Flight Data Applying Extended and Unscented Kalman Filter. *Aerospace Science and Technology*, Vol. 14, 2010, pp.106-117.
- [5] Han, P., Gan, H., He W., Alazard, D., and Defay, F., Aircraft attitude estimation based on central difference Kalman filter. *11th International Conference on Signal Processing (ICSP 2012)*, Oct 2012, pp.294-298.
- [6] Kaba, A., Unscented Kalman filter based attitude estimation of a quadrotor, *Journal of Aeronautics and Space Technologies*, Vol. 14, No. 1, 2021, pp.79-84.
- [7] Erkeç, T. Y. and Hajiyev, C., Review on Relative Navigation Methods of Space Vehicles. *Current Chinese Science*, 2020.
- [8] Gao, W., Miao, L., and Ni, M., Multiple Fading Factors Kalman Filter for SINS Static Alignment Application, *Chinese Journal of Aeronautics*, Vol. 24, 2011, pp.476-483.
- [9] Zeng, Zhankui & Zhang, Shijie & Xing, Yanjun & Cao, Xibin. (2014). Robust Adaptive Filter for Small Satellite Attitude Estimation Based on Magnetometer and Gyro. *Abstract and Applied Analysis*. 2014. pp.1-7.
- [10] Almagbile, A., Wang, J. & Al-Rawabdeh, A., An integrated adaptive Kalman filter for improving the reliability of navigation

- systems. *Journal of Applied Geodesy*, Vol. 17(3), 2023, pp.295-311.
- [11] Pan, H., Gao, J., Li, Z., Qian, N., Li, F., Multiple fading factors-based strong tracking variational Bayesian adaptive Kalman filter, *Measurement*, Vol. 176, 2021.
- [12] Mclean, D., *Automatic Flight Control Systems*, Hertfordshire, Prentice Hall International, 1990.
- [13] Hacıyev, Ç., *Experiment Data Processing Methods, and Engineering Applications*, Nobel Publishing, 2010.
- [14] Akhlaghi, S., Zhou, N., and Huang, Z., Adaptive adjustment of noise covariance in Kalman filter for dynamic state estimation, *IEEE Power & Energy Society General Meeting*, 2017, pp.1-5.
- [15] Hajiyev C., and Soken E., Robust Estimation of UAV Dynamics in the Presence of Measurement Faults, *Journal of Aerospace Engineering*, Vol. 25, No. 1, 2012, pp.80-89.
- [16] Sever, M., Erkeç, T.Y. and Hajiyev, C., Aircraft State Estimation via KF&AKF Methods. *Proceedings of 10 International Conference on Recent Advances in Air and Space Technologies*, June 7-9, 2023, Istanbul, Turkey.

Contribution of Individual Authors to the Creation of a Scientific Article (Ghostwriting Policy)

The authors equally contributed in the present research, at all stages from the formulation of the problem to the final findings and solution.

Sources of Funding for Research Presented in a Scientific Article or Scientific Article Itself

No funding was received for conducting this study.

Conflict of Interest

The authors have no conflict of interest to declare.

Creative Commons Attribution License 4.0 (Attribution 4.0 International, CC BY 4.0)

This article is published under the terms of the Creative Commons Attribution License 4.0

https://creativecommons.org/licenses/by/4.0/deed.en_US